



Chair for Multiscale Simulation
Friedrich-Alexander-Universität
Erlangen-Nürnberg



MASTER THESIS

Probing quasi static force models for the interaction for the interaction of granular particles

SANJAY CHAMOLI

Erlangen, September 30, 2016

Examiner: Prof. Dr. Thorsten Pöschel
Advisor: Dr. Patric Müller

Eidesstattliche Erklärung / Statutory Declaration

Hiermit versichere ich eidesstattlich, dass die vorliegende Arbeit von mir selbständig, ohne Hilfe Dritter und ausschließlich unter Verwendung der angegebenen Quellen angefertigt wurde. Alle Stellen, die wörtlich oder sinngemäß aus den Quellen entnommen sind, habe ich als solche kenntlich gemacht. Die Arbeit wurde bisher in gleicher oder ähnlicher Form keiner anderen Prüfungsbehörde vorgelegt.

I hereby declare formally that I have developed and written the enclosed thesis entirely by myself and have not used sources or means without declaration in the text. Any thoughts or quotations which were inferred from the sources are marked as such. This thesis was not submitted in the same or a substantially similar version to any other authority to achieve an academic grading.

Der Friedrich-Alexander-Universität, vertreten durch den Lehrstuhl für Multiscale simulation, wird für Zwecke der Forschung und Lehre ein einfaches, kostenloses, zeitlich und örtlich unbeschränktes Nutzungsrecht an den Arbeitsergebnissen der Arbeit einschließlich etwaiger Schutz- und Urheberrechte eingeräumt.

Erlangen, September 30, 2016

SANJAY CHAMOLI

Abstract

An important model for granular particles are elastic and viscoelastic spheres. The macroscopic interaction forces for such objects are commonly obtained from the continuum mechanical equations of motion for elastic and viscoelastic material in quasi static approximation. The same holds true for the coefficients of restitution of colliding spheres which are, in turn, obtained from the macroscopic interaction forces. The quasi static assumption implies that the characteristic deformation rate is much smaller than the speed of sound in the material and that the relaxation time of the particle's material is negligible compared to the duration of the contact. In this work the validity of these assumptions is probed for realistic impact scenarios by comparing to a direct numerical solution of the underlying continuum mechanical equations of motion by means of finite elements.

Acknowledgments

I would like to express my sincere gratitude to my advisor Dr. Patric Müller and Prof. Dr. Thorsten Pöschel for their continuous support, patience, motivation, and immense knowledge. Their guidance helped me in all the time of research and writing of this thesis.

I would also like to thank my family and friends, for all their love and support.

List of Figures

1.1	Hertz Problem	3
2.1	Three tension tests are assumed to be carried out along x, y, z , respectively, and strains superposed.	11
2.2	Configurations of body in motion	13
2.3	Mesh	17
2.4	Bottom Half of Mesh	18
2.5	Rigid Plane	18
2.6	Assembly	19
2.7	Center of sphere	20
3.1	A very soft material	22
3.2	Contact force vs Time for various impact velocities	23
3.3	Displacement of the center of the sphere for various impact velocities	24
3.4	Kinetic Energy	25
3.5	Kinetic Energy contact after impact	25
3.6	Strain Energy	26
3.7	Strain Energy after contact is broken	26
3.8	Coefficient of restitution	27
3.9	Different modes of vibration	28
3.10	Fourier Transform of Strain Energy	30
3.11	Number of oscillation during contact	30
3.12	Coefficient of restitution for various Young's Modulus	31
3.13	Coefficient of restitution for various radii	32

CONTENTS

1	Introduction	1
1.1	Granular Material	1
1.2	Particle Simulations of Granulates	2
1.2.1	Why to simulate?	2
1.2.2	Methods of simulation	2
1.3	Particle Models	3
1.4	Aims	8
2	Simulation Method	9
2.1	FEM	9
2.1.1	Steps in FEM	9
2.1.2	Constitutive Laws	10
2.2	Simulation Setup	16
2.2.1	Sphere vs Rigid Plane	16
2.2.2	Symmetry	16
2.2.3	Mesh	17
2.2.4	Rigid Plane	18
2.2.5	Assembly	18
2.3	Measurement Quantities	19
2.3.1	Displacement	19
2.3.2	Kinetic Energy	19
2.3.3	Strain Energy	19
2.3.4	Coefficient of Restitution	20
2.4	Verification	20
3	Results	21
3.1	Results	21
3.1.1	Contact Force	23
3.1.2	Deformation	24
3.1.3	Energy	25
3.1.4	Coefficient of Restitution	27
3.1.5	Modal Analysis	28
3.2	Parametric Study	31
3.2.1	Different Young's Modulus	31
3.2.2	Different Diameters	32

4 Conclusion and Future Work	33
4.1 Summary	33
4.2 Future Work	34
Bibliography	35

1

INTRODUCTION

1.1 Granular Material



(a) Hourglass



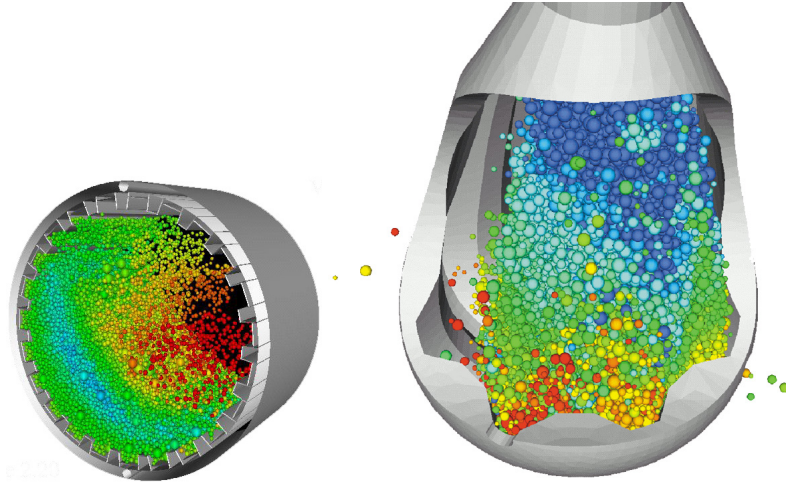
(b) Heap of Sand

A granular material is a conglomeration of discrete solid, macroscopic particles characterized by a loss of energy whenever the particles interact (the most common example would be friction when grains collide). The constituents that compose granular material must be large enough such that they are not subject to thermal motion fluctuations. Thus, the lower size limit for grains in granular material is about $1\mu m$. On the upper size limit, the physics of granular materials may be applied to ice floes where the individual grains are icebergs and to asteroid belts of the Solar System with individual grains being asteroids. [1]

Granular materials are very important in many industrial processes, in natural sciences and everyday life. A peculiar characteristic of granular materials is that, they behave differently under different circumstances. For example, they behave like fluids while flowing in an hour glass and pipes, whereas a heap of sand does not flow and behaves like a solid. The same heap of sand can deform plastically if some force is applied on it.

1.2 Particle Simulations of Granulates

1.2.1 Why to simulate?



There are many reasons to simulate granular materials [6]. Conducting experiments with engineering devices are generally time consuming, dangerous and expensive, as they require specialized equipment. They are extensively used in industries and are an important part of everyday life. Since there is no comprehensive theory on granular materials which reliably predict the behavior of such materials in technical devices, numerical simulations can be used to predict and to optimize the function of machinery in powder technology before the machine is built. Hence it makes sense to use the power of computers to simulate granular material.

1.2.2 Methods of simulation

A few of the models used in simulation of granular materials are

Force Based Model

In this model, the general idea is to solve numerically Newton's equations of motion.

- **Rigid Body dynamics** The interaction forces are determined from consistency requirements on the behavior of the particles. This method is therefore suited to simulate perfectly rigid particles without the necessity to specify a certain deformation law.
- **Molecular Dynamics** In the most common version, the trajectories of granulates are determined by numerically solving Newton's equations of motion for a system of interacting granulates. Here the Newton's equation of motion is solved simultaneously for all particles i :

$$\ddot{\vec{r}}_i = \frac{1}{m_i} \vec{F}_i(\vec{r}_1, \vec{v}_1, \dots, \vec{r}_N, \vec{v}_N)$$

- **Discrete Element Method**

DEMs are closely related to Molecular Dynamics, but also includes rotational degrees-of-freedom as well as stateful contact and often complicated geometries. Discrete Elements methods are generally computationally intensive, therefore limiting the length of a simulation or number of particles.

Event Driven Model

In Event Driven Models, the flow of the algorithm is determined by events such as collisions in the case of simulation of granular materials. The trajectory and velocity of granulates after collisions is determined with factors such as coefficient of restitution.

1.3 Particle Models

Hertz Theory [2]

The oldest and most influential model of contacts mechanics which can be used in force based models is the Hertz contact theory. In Hertz's classical theory of contact, he focused primarily on non-adhesive contact where no tension force is allowed to occur within the contact area. The following assumptions are made in determining the solutions of Hertzian contact problems:

- The strains are small and within the elastic limit.
- Each body can be considered an elastic half-space, i.e., the area of contact is much smaller than the characteristic radius of the body.
- The surfaces are continuous and non-conforming.
- The bodies are in frictionless contact.

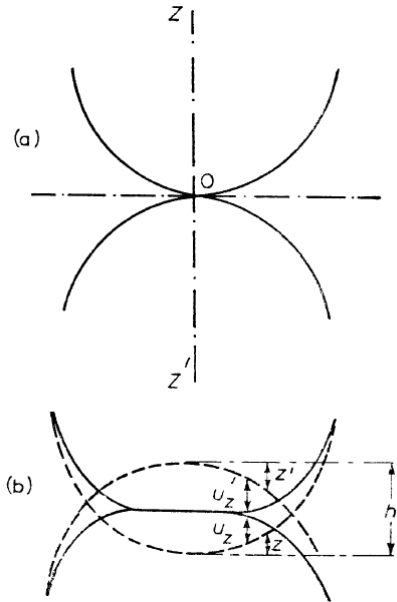


Figure 1.1: Hertz Problem

Let two solid bodies be in contact at a point which is not a singular point on either surface. Figure 1.1 shows a cross-section of the two surfaces near the point of contact O . The surfaces have a common tangent plane at O , which we take as the xy -plane. We regard the positive z -direction as being into either body (i.e. in opposite directions for the two bodies) and denote the corresponding co-ordinates by z and z' .

Near a point of ordinary contact with the xy -plane, the equation of the surface can be written

$$z = \kappa_{\alpha\beta} x_\alpha x_\beta \quad (1.1)$$

where summation is understood over the values 1, 2, of the repeated suffixes $\alpha, \beta(x_1 - x, x; = y)$, and $\kappa_{\alpha\beta}$ is a symmetrical tensor of rank two, which characterizes the curvature of the surface: the principal values of the tensor $\kappa_{\alpha\beta}$ are $\frac{1}{2R_1}$ and $\frac{1}{2R_2}$, where R and R_2 are the principal radii of curvature of the surface at the point of contact. A similar relation for the surface of the other body near the point of contact can be written

$$z' = \kappa'_{\alpha\beta} x_\alpha x_{\beta\alpha} \quad (1.2)$$

Let us now assume that the two bodies are pressed together by applied forces, and approach a short distance h (*Hertz's problem*). The deformation occurs near the original point of contact, and the two bodies will be in contact over a small but finite portion of their surfaces. Let u , and u' , be the components (along the z and z' axes respectively) of the corresponding displacement vectors for points on the surfaces of the two bodies. The broken lines in figure 1.1 show the surfaces as they would be in the absence of any deformation, while the continuous lines show the surfaces of the deformed bodies; the letters z and z' denote the distances given by equations 1.1 and 1.2. It is seen at once from the figure that the equation

$$(z + u_z) + (z' + u'_z) = h \quad (1.3)$$

or

$$(\kappa_{\alpha\beta} x_\alpha x_{\beta\alpha} + \kappa'_{\alpha\beta} x_\alpha x_{\beta\alpha}) \quad (1.4)$$

holds everywhere in the region of contact. At points outside the region of contact, we have

$$z + z' + u_z + u'_z > h \quad (1.5)$$

We choose the x and y axes to be the principal axes of the tensor $\kappa_{\alpha\beta} + \kappa'_{\alpha\beta}$. Denoting the principal values of this tensor by A and B , we can rewrite equation 1.4 as

$$Ax_2 + By_2 + u_z + u'_z = h \quad (1.6)$$

We denote by $P_z(x, y)$ the pressure between the two deformed bodies at points in the region of contact; outside this region, of course $P_z = 0$. To determine the relation between P_z and the displacements u_z, u'_z , we can with sufficient accuracy regard the surfaces as plane and use the formula [2].

$$\begin{aligned} u_x &= \frac{1+\sigma}{2\pi E} \frac{1}{r} \left\{ -\frac{(1-2\sigma)x}{r} F_z + 2(1-\sigma)F_x + \frac{2\sigma x}{r^2} (xF_x + yF_y) \right\} \\ u_y &= \frac{1+\sigma}{2\pi E} \frac{1}{r} \left\{ -\frac{(1-2\sigma)y}{r} F_z + 2(1-\sigma)F_y + \frac{2\sigma y}{r^2} (xF_x + yF_y) \right\} \\ u_z &= \frac{1+\sigma}{2\pi E} \frac{1}{r} \left\{ 2(1-\sigma)F_z + \frac{2\sigma y}{r} (xF_x + yF_y) \right\} \end{aligned} \quad (1.7)$$

$$u_i = \int \int G_{ik}(x - x', y - y', z) P_k(x', y') dx' dy' \quad (1.8)$$

According to the third of formulae 1.7 and 1.8, the displacement u , under the action of normal forces $P_z(x, y)$ is given by

$$\begin{aligned} u_z &= \frac{1-\sigma^2}{\pi E} \int \int \frac{P_z(x', y')}{r} dx' dy' \\ u'_z &= \frac{1-\sigma'^2}{\pi E'} \int \int \frac{P_z(x', y')}{r} dx' dy' \end{aligned} \quad (1.9)$$

where a, a' and E, E' are the Poisson's ratios and the Young's moduli of the two bodies. Since $P = 0$

outside the region of contact, the integration extends only over this region. It may be noted that, from these formulae, the ratio $\frac{u_z}{u'_z}$ is constant:

$$\frac{u_z}{u'_z} = \frac{(1 - \sigma^2)E'}{(1 - \sigma'^2)E} \quad (1.10)$$

The relations 1.6 and 1.10 together give the displacements in u_z , u'_z at every point of the region of contact (although 1.9 and 1.10, of course, relate to points outside that region also).

Substituting the expressions 1.9 in 1.6, we obtain

$$\frac{1}{\pi} \left(\frac{1 - \sigma^2}{E} + \frac{1 - \sigma'^2}{E'} \right) \int \int \frac{P_z(x', y')}{r} dx' dy' = h - Ax^2 - By^2 \quad (1.11)$$

This integral equation determines the distribution of the pressure P_z over the region of contact. Its solution can be found by analogy with the following results of potential theory. The idea of using this analogy arises as follows: firstly, the integral on the left-hand side of equation 1.11 is of type commonly found in potential theory, where such integrals give the potential of a charge distribution; secondly, the potential inside a uniformly charged ellipsoid is a quadratic function of the co-ordinates.

If the ellipsoid $\frac{x^2}{a^2} + \frac{y^2}{b^2} + \frac{z^2}{c^2}$ is uniformly charged (with volume charged density σ), the potential in the ellipsoid is given by

$$\phi(x, y, z) = \pi \sigma abc \int_{\infty}^0 \left\{ 1 - \frac{x^2}{a^2 + \xi} - \frac{y^2}{b^2 + \xi} - \frac{z^2}{c^2 + \xi} \right\} \frac{d\xi}{\sqrt{(a^2 + \xi)(b^2 + \xi)(c^2 + \xi)}} \quad (1.12)$$

In the limiting case of an ellipsoid which is very much flattened in the z -direction ($c \rightarrow 0$), we have

$$\phi(x, y) = \pi \sigma abc \int_{\infty}^0 \left\{ 1 - \frac{x^2}{a^2 + \xi} - \frac{y^2}{b^2 + \xi} \right\} \frac{d\xi}{\sqrt{(a^2 + \xi)(b^2 + \xi)\xi}} \quad (1.13)$$

in passing to the limit ($c \rightarrow 0$) we must of course put $z = 0$ for points inside the ellipsoid. The potential $\phi(x, y, z)$ also be written as

$$\phi(x, y, z) = \int \int \int \frac{\rho dx' dy' dz'}{\sqrt{(x - x')^2 + (y - y')^2 + (z - z')^2}} \quad (1.14)$$

where the integration is over the volume of the ellipsoid. In pasing to the limit ($c \rightarrow 0$), we must put $z = z' = 0$ in the radicand; integrating over z' between the limits

$$\pm c \sqrt{\left\{ 1 - \left(\frac{x'^2}{a^2} \right) - \left(\frac{y'^2}{b^2} \right) \right\}} \quad (1.15)$$

we obtain

$$\phi(x, y) = 2\rho c \int \int \frac{dx' dy'}{r} \sqrt{\left(1 - \frac{x'^2}{a^2} - \frac{y'^2}{b^2} \right)} \quad (1.16)$$

where

$$r = \sqrt{(x - x')^2 + (y - y')^2} \quad (1.17)$$

and the integration is over the area inside the ellipse

$$\frac{x'^2}{a^2} + \frac{y'^2}{b^2} = 1 \quad (1.18)$$

Equating the two expressions for $\phi(x, y)$, we obtain the identity

$$\int \int \frac{dx' dy'}{r} \sqrt{\left(1 - \frac{x'^2}{a^2 - \frac{y'^2}{b^2}}\right)} = \frac{1}{2} \pi ab \int_{\infty}^0 \left(1 - \frac{x^2}{a^2 + \xi} - \frac{y^2}{b^2 + \xi}\right) \frac{d\xi}{\sqrt{(a^2 + \xi)(b^2 + \xi)\xi}} \quad (1.19)$$

Comparing this relation with equation 1.11, we see that the right-hand sides are quadratic functions of x and y of the same form, and the left-hand sides are integrals of the same form. We can therefore deduce immediately that the region of contact (i.e. the region of integration in 1.11) is bounded by an ellipse of the form

$$\frac{x^2}{a^2} + \frac{y^2}{b^2} = 1 \quad (1.20)$$

and that the function $P_z(x, y)$ must be of the form

$$P_z(x, y) = \text{constant} \times \sqrt{\left(1 - \frac{x^2}{a^2} - \frac{y^2}{b^2}\right)} \quad (1.21)$$

Taking the constant such that the integral $\int \int P_z dx dy$ over the region of contact is equal to the given total force F which moves the bodies together, we obtain

$$P_z(x, y) = \frac{3F}{2\pi ab} \sqrt{\left(1 - \frac{x^2}{a^2} - \frac{y^2}{b^2}\right)} \quad (1.22)$$

This formula gives the distribution of pressure over the tree of the region of contact. It may be pointed out that the pressure at the centre of this region is $\frac{3}{2}$ times the mean pressure $\frac{F}{\pi ab}$.

Substituting 1.22 in equation 1.11 and replacing the resulting integral in accordance with 1.19, we obtain

$$\frac{FD}{\pi} \int_{\infty}^0 \left(1 - \frac{x^2}{a^2 + \xi} - \frac{y^2}{b^2 + \xi}\right) \frac{d\xi}{\sqrt{(a^2 + \xi)(b^2 + \xi)\xi}} = h - Ax^2 - By^2 \quad (1.23)$$

where

$$D = \frac{3}{4} \left(\frac{1 - \sigma^2}{E} + \frac{1 - \sigma'^2}{E'} \right)$$

This equation must hold identically for all values of x and y inside the ellipse 1.20; the coefficients of x and y and the free terms must therefore be respectively equal on each side. Hence we find

$$h = \frac{FD}{\pi} \int_{\infty}^0 \frac{d\xi}{\sqrt{(a^2 + \xi)(b^2 + \xi)\xi}} \quad (1.24)$$

$$\begin{aligned} A &= \frac{FD}{\pi} \int_{\infty}^0 \frac{d\xi}{(a^2 + \xi)\sqrt{(a^2 + \xi)(b^2 + \xi)\xi}} \\ B &= \frac{FD}{\pi} \int_{\infty}^0 \frac{d\xi}{(b^2 + \xi)\sqrt{(a^2 + \xi)(b^2 + \xi)\xi}} \end{aligned} \quad (1.25)$$

Equations 1.25 determine the semi-axes a and b of the region of contact from the given force F (A and B being known for given bodies). The relation 1.24 then gives the distance of approach h as a function of the force F . The right-hand sides of these equations involve elliptic integrals.

Thus the problem of bodies in contact can be regarded as completely solved. The form of the surfaces (i.e. the displacements u_z, u'_z) outside the region of contact is determined by the same formulae 1.9 and 1.22;

the values of the integrals can be found immediately from the analogy with the potential outside a charged ellipsoid. Finally, the formulae 1.7 enable us to find also the deformation at various points in the bodies (but only, of course, at distances small compared with the dimensions of the bodies).

Let us apply these formulae to the case of contact between two spheres of radii R and R' . Here $A = B = \frac{1}{2R} + \frac{1}{2R'}$. It is clear from symmetry that $a = b$, i.e. the region of contact is a circle. From 1.25 we find the radius a of this circle to be

$$a = F^{\frac{1}{3}} \left(\frac{DRR'}{R + R'} \right)^{\frac{1}{3}} \quad (1.26)$$

h is in this case the difference between the sum $R + R'$ and the distance between the centres of the spheres. From 1.22 we obtain the following relation between F and h :

$$h = F^{\frac{1}{3}} \left[D^2 \left(\frac{1}{R} + \frac{1}{R'} \right) \right]^{\frac{1}{3}} \quad (1.27)$$

It should be noticed that h is proportional to $F^{\frac{2}{3}}$; conversely, the force F varies as $h^{\frac{3}{2}}$. We can write down also the potential energy U of the spheres in contact. Since $-F = -\frac{\partial U}{\partial h}$, we have

$$U = h^{\frac{5}{2}} \frac{2}{5D} \sqrt{\frac{RR'}{R + R'}} \quad (1.28)$$

Finally, it may be mentioned that a relation of the form $h = \text{constant} \times F^{\frac{2}{3}}$ or $F = \text{constant} \times h^{\frac{3}{2}}$, holds not only for spheres but also for other finite bodies in contact. This is easily seen from similarity arguments. If we make the substitution

$$a^2 \rightarrow \alpha a^2, \quad b^2 \rightarrow \alpha b^2, \quad F \rightarrow \alpha^{\frac{3}{2}} F$$

where α is an arbitrary constant, equations (9.12) remain In equation 1.24, the right-hand side is multiplied by α , and so h must be replaced by αh if this equation is to remain unchanged. Hence it follows that F must be proportional to $h^{\frac{3}{2}}$.

Collision of two spheres

Consider a system of coordinates in which the center of mass of the two spheres is at rest, the energy before the collision is equal to the kinetic energy of the relative motion $\frac{1}{2}mv^2$, where v is the relative velocity of the colliding spheres and $\mu = \frac{m_1 m_2}{m_1 + m_2}$ their reduced mass. During the collision, the total energy is the sum of the kinetic energy, which may be written $\frac{1}{2}\mu h^2$, and the potential energy 1.28. By, the law of conservation of energy we have

$$\mu \left(\frac{dh}{dt} \right)^2 + kh^{\frac{5}{2}} = \mu v^2, \quad k = \frac{4}{5D} \sqrt{\frac{RR'}{R + R'}} \quad (1.29)$$

The maximum approach h_0 of the spheres corresponds to the time when their relative velocity $h = 0$, and is $h_0 = (\frac{\mu}{k})^{\frac{2}{5}} v^{\frac{4}{5}}$. The time τ during which the collision takes place (i.e. h varies from 0 to h_0 and back is

$$\tau = 2 \int_{h_0}^0 \frac{dh}{\sqrt{v^2 - \frac{kh^{\frac{5}{2}}}{\mu}}} = 2 \left(\frac{\mu^2}{k^2 v} \right)^{\frac{1}{5}} \int_1^0 \frac{dx}{\sqrt{1 - x^{\frac{2}{5}}}} = 2.94 \left(\frac{\mu^2}{k^2 v} \right)^{\frac{1}{5}} \quad (1.30)$$

By using the statical formulae obtained to solve the this problem, we have neglected elastic oscillations of

the spheres resulting from the collision. If this is legitimate, the velocity v must be small compared with the velocity of sound.

Collision of a sphere with a rigid plane

The case of a sphere colliding with a plane can be approximated as collision of two spheres, where one sphere has a radius of ∞ and mass also of ∞ . Therefore using 1.30 with m_1 as mass of the sphere, $m_2 = \infty$ as mass of the plane, R_1 as radius of the sphere and $R_2 = \infty$ as radius of the plane.

Substituting $E' = \infty$ in 1.23

$$D = \frac{3}{4} \left(\frac{1 - \sigma}{E} \right)$$

From 1.29

$$\begin{aligned} k &= \frac{4}{5D} \sqrt{\frac{R_1 R_2}{R_1 + R_2}} = \frac{4}{5D} \sqrt{\frac{R_1}{\frac{R_1}{R_2} + 1}} \\ k &= \frac{4}{5D} \sqrt{R_1} \\ k &= \frac{16E}{5(1 - \sigma)} \sqrt{R_1} \end{aligned}$$

now $\mu = \frac{m_1 m_2}{m_1 + m_2} = m_1$

substituting the above values in 1.30 and considering $m_1 = \frac{4}{3}\pi R_1^3$

$$\begin{aligned} \tau &= 2.94 \left(\frac{\mu^2}{k^2 v} \right)^{\frac{1}{5}} \\ \tau &= 2.94 R_1 v^{\frac{1}{5}} \left(\frac{5\pi\rho(1 - \sigma)}{12E} \right)^{\frac{2}{5}} \end{aligned}$$

1.4 Aims

The aim of this thesis is to check validity of quasi static assumptions by considering the collision of two spheres of same material and radius. The quasi-static approximation implies that

- The characteristic deformation rate is much smaller than the speed of sound in the system.
- The microscopic relaxation time of the particle's material is negligibly small as compared to the duration of the impact.

One way to validate the approximations is by calculating the coefficient of restitution of the sphere for various impact velocities. The coefficient of restitution would also give an idea of the conversion of kinetic energy to vibrations after impact is complete, which is ignored by the quasi static assumptions.

2

SIMULATION METHOD

2.1 FEM

The finite element method (FEM) is a numerical technique for solving problems which are described by partial differential equations or can be formulated as functional minimization. A domain of interest is divided into an assembly of finite elements. Approximating functions in finite elements are determined in terms of nodal values of a physical field which is sought. A continuous physical problem is transformed into a discretized finite element problem with unknown nodal values. For a linear problem a system of linear algebraic equations should be solved. Values inside finite elements can be recovered using nodal values. FEM then uses variational methods from the calculus of variations to approximate a solution by minimizing an associated error function. Two features of the FEM are worth to be mentioned:

- Piece-wise approximation of physical fields on finite elements provides good precision even with simple approximating functions (increasing the number of elements we can achieve any precision).
- Locality of approximation leads to sparse equation systems for a discretized problem. This helps to solve problems with very large number of nodal unknowns.

2.1.1 Steps in FEM

Finite Element Method can be generalized into these steps.

- The physical problem has to be defined. All the desired results and the geometry of the problem have to be specified.
- The mathematical model has to be formulated. The physical problem has to be formulated as an (initial) boundary value problem, e.g. by means of partial differential equations with boundary and, if required, initial conditions.
- The FE model has to be setup, which means that the mathematical model has to be discretised and the equations are solved. The structure is subdivided into finite elements, the solution is approxi-

mated element-wise and computed at the nodes of these elements. By this procedure, the differential equations are transferred into a system of algebraic equations

$$K.u = F \quad (2.1)$$

For a static stress analysis, the unknown nodal values subsumed in u are the nodal displacements, K is the stiffness matrix and f contains the nodal forces. This system of equations has to be solved for the unknown nodal values

$$u = K^{-1} \cdot f \quad (2.2)$$

Subsequently, the dependent variables have to be computed in a so-called post-processing step. For a stress analysis the strains, the stresses, equivalent stresses and further variables are derived from the nodal displacement values and are usually displayed graphically.

- The FE model yields a numerical solution which is an approximation of the exact solution of the mathematical problem. It has to be verified that the numerical solution is accurate enough and, if not, the FE model has to be improved. A more accurate solution can be obtained by choosing a larger number of nodes, which results in smaller finite elements. This, however, leads to higher computational effort such that an FE solution always represents a reasonable compromise between accuracy and computational effort.
- When a satisfying numerical solution is found, the results have to be interpreted and validated. This is usually done by comparing them to those obtained from experiments. If the numerical solution does not sufficiently capture the relevant phenomena, the physical problem or the mathematical model might have to be adapted. The comparison between numerical and experimental results can also be used to e.g. identify material parameters.

2.1.2 Constitutive Laws

Elastic Modulus and Poisson's Ratio In 1D Stress State The one-dimensional Hooke's law relates 1D normal stress to 1D extensional strain through two material parameters the modulus of elasticity E , also called Young's modulus and Poisson's ratio ν . The modulus of elasticity connects axial stress σ to axial strain ϵ :

$$\sigma = E\epsilon \quad (2.3)$$

Poisson's ratio ν is defined as ratio of lateral strain to axial strain:

$$\nu = \left| \frac{\text{lateral strain}}{\text{axial strain}} \right| = -\frac{\text{lateral strain}}{\text{axial strain}} \quad (2.4)$$

The $-$ sign is introduced for convenience so that ν comes out positive. For structural materials ν lies in the range $0.0 \leq \nu < 0.5$. For most metals $\nu \approx 0.25-0.35$. For concrete and ceramics, $\nu \approx 0.10$. For cork $\nu \approx 0$. For rubber, $\nu \approx 0.5$ to 3 places. A material for which $\nu = 0.5$ is called incompressible.

Shear Modulus In 1D Stress State

The shear modulus G connects a shear strain γ to the corresponding shear stress τ :

$$\tau = G\gamma \quad (2.5)$$

"Corresponding" means that if $\gamma = \gamma_{xy}$, say, then $\tau = \tau_{xy}$, and similarly for the other shear components. The shear modulus is usually obtained from a torsion test. It turns out that the 3 material properties E, τ

and G for an elastic isotropic material are not independent, but are connected by the relations

$$G = \frac{E}{2(1 + \nu)} \quad (2.6)$$

which means that if two of them are known by measurement, the third one can be obtained from the relations 2.6. In practice the three properties are often measured independently, and the (approximate) verification of 2.6 gives an idea of how isotropic the material is.

Shear Modulus In 3D Stress State

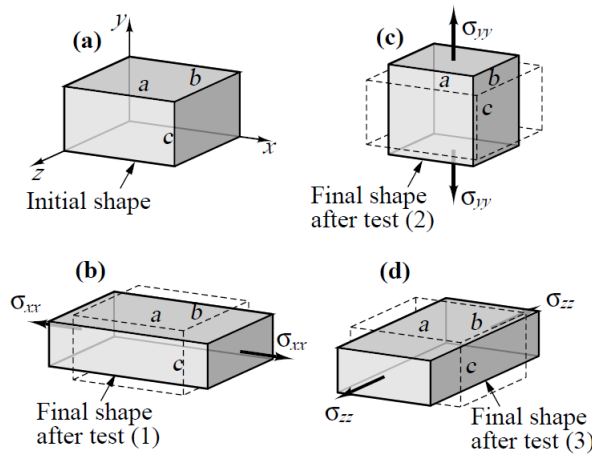


Figure 2.1: Three tension tests are assumed to be carried out along x , y , z , respectively, and strains superposed.

We now generalize the foregoing equations to the three-dimensional case, still assuming that the material is elastic and isotropic. Consider a cube of material aligned with the axes x , y , z , as shown in figure 2.1. Imagine that three tension tests, labeled (1), (2) and (3) respectively, are conducted along x , y and z , respectively. Pulling the material by applying σ_{xx} along x will produce normal strains

$$\epsilon_{xx}^{(1)} = \frac{\sigma_{xx}}{E}, \quad \epsilon_{yy}^{(1)} = -\frac{\nu\sigma_{xx}}{E}, \quad \epsilon_{zz}^{(1)} = -\frac{\nu\sigma_{xx}}{E} \quad (2.7)$$

Next, pull the material by σ_{yy} along y to get the strains

$$\epsilon_{xx}^{(2)} = \frac{\nu\sigma_{yy}}{E}, \quad \epsilon_{yy}^{(2)} = -\frac{\sigma_{yy}}{E}, \quad \epsilon_{zz}^{(2)} = -\frac{\nu\sigma_{yy}}{E} \quad (2.8)$$

Finally pull the material by σ_{zz} along z to get

$$\epsilon_{xx}^{(3)} = \frac{\nu\sigma_{zz}}{E}, \quad \epsilon_{yy}^{(3)} = -\frac{\nu\sigma_{zz}}{E}, \quad \epsilon_{zz}^{(3)} = -\frac{\sigma_{zz}}{E} \quad (2.9)$$

In the general case the cube is subjected to combined normal stresses σ_{xx} , σ_{yy} and σ_{zz} . Since we assumed that the material is linearly elastic, the combined strains can be obtained by superposition of the foregoing results:

$$\begin{aligned}\epsilon_{xx} &= \epsilon_{xx}^{(1)} + \nu\epsilon_{yy}^{(2)} + \nu\epsilon_{zz}^{(3)} = \frac{\sigma_{xx}}{E} - \frac{\nu\sigma_{yy}}{E} - \frac{\nu\sigma_{zz}}{E} = \frac{1}{E}(\sigma_{xx} - \nu\sigma_{yy} - \nu\sigma_{zz}) \\ \epsilon_{yy} &= -\nu\epsilon_{xx}^{(1)} + \epsilon_{yy}^{(2)} + \nu\epsilon_{zz}^{(3)} = \frac{-\nu\sigma_{xx}}{E} + \frac{\nu\sigma_{yy}}{E} - \frac{\nu\sigma_{zz}}{E} = \frac{1}{E}(-\sigma_{xx} + \nu\sigma_{yy} - \nu\sigma_{zz}) \\ \epsilon_{zz} &= -\nu\epsilon_{xx}^{(1)} + \nu\epsilon_{yy}^{(2)} - \epsilon_{zz}^{(3)} = \frac{-\nu\sigma_{xx}}{E} - \frac{\nu\sigma_{yy}}{E} + \frac{\nu\sigma_{zz}}{E} = \frac{1}{E}(-\nu\sigma_{xx} - \nu\sigma_{yy} + \sigma_{zz})\end{aligned}\quad (2.10)$$

The shear strains and stresses are connected by the shear modulus as

$$\gamma_{xy} = \gamma_{yx} = \frac{\tau_{xy}}{G} = \frac{yx}{G}, \quad \gamma_{yz} = \gamma_{zy} = \frac{\tau_{yz}}{G} = \frac{zy}{G}, \quad \gamma_{zx} = \gamma_{xz} = \frac{\tau_{zx}}{G} = \frac{xz}{G} \quad (2.11)$$

The equation 2.10 and 2.11, can be expressed in matrix form

$$\begin{bmatrix} \epsilon_{xx} \\ \epsilon_{yy} \\ \epsilon_{zz} \\ \gamma_{xy} \\ \gamma_{yz} \\ \gamma_{zx} \end{bmatrix} = \begin{bmatrix} \frac{1}{E} & -\frac{\nu}{E} & -\frac{\nu}{E} & 0 & 0 & 0 \\ -\frac{\nu}{E} & \frac{1}{E} & -\frac{\nu}{E} & 0 & 0 & 0 \\ -\frac{\nu}{E} & -\frac{\nu}{E} & \frac{1}{E} & 0 & 0 & 0 \\ 0 & 0 & 0 & \frac{1}{G} & 0 & 0 \\ 0 & 0 & 0 & 0 & \frac{1}{G} & 0 \\ 0 & 0 & 0 & 0 & 0 & \frac{1}{G} \end{bmatrix} \begin{bmatrix} \sigma_{xx} \\ \sigma_{yy} \\ \sigma_{zz} \\ \tau_{xy} \\ \tau_{yz} \\ \tau_{zx} \end{bmatrix} \quad (2.12)$$

Stress Strain Relation

To get stresses if the strains are given, the most expedient method is to invert the matrix equation 2.12. This gives

$$\begin{bmatrix} \sigma_{xx} \\ \sigma_{yy} \\ \sigma_{zz} \\ \tau_{xy} \\ \tau_{yz} \\ \tau_{zx} \end{bmatrix} = \begin{bmatrix} \hat{E}(1-\nu) & \hat{E}\nu & \hat{E}\nu & 0 & 0 & 0 \\ \hat{E}\nu & \hat{E}(1-\nu) & \hat{E}\nu & 0 & 0 & 0 \\ \hat{E}\nu & \hat{E}\nu & \hat{E}(1-\nu) & 0 & 0 & 0 \\ 0 & 0 & 0 & G & 0 & 0 \\ 0 & 0 & 0 & 0 & G & 0 \\ 0 & 0 & 0 & 0 & 0 & G \end{bmatrix} \begin{bmatrix} \epsilon_{xx} \\ \epsilon_{yy} \\ \epsilon_{zz} \\ \gamma_{xy} \\ \gamma_{yz} \\ \gamma_{zx} \end{bmatrix} \quad (2.13)$$

Here \hat{E} is an effective modulus modified by Poisson's ratio:

$$\hat{E} = \frac{E}{(1-2\nu)(1+\nu)} \quad (2.14)$$

The matrix 2.13 written in long form is:

$$\begin{aligned}\sigma_{xx} &= \frac{E}{(1-2\nu)(1+\nu)}[(1-\nu)\epsilon_{xx} + \nu\epsilon_{yy} + \nu\epsilon_{zz}] \\ \sigma_{yy} &= \frac{E}{(1-2\nu)(1+\nu)}[\nu\epsilon_{xx} + (1-\nu)\epsilon_{yy} + \nu\epsilon_{zz}] \\ \sigma_{zz} &= \frac{E}{(1-2\nu)(1+\nu)}[\nu\epsilon_{xx} + \nu\epsilon_{yy} + (1-\nu)\epsilon_{zz}] \\ \tau_{xy} &= G\gamma_{xy}, \quad \tau_{yz} = G\gamma_{yz}, \quad \tau_{zx} = G\gamma_{zx}\end{aligned}\quad (2.15)$$

Kinematics [4]

The basic variables to describe the motion and deformation flexible bodies are Deformation, Velocity and Acceleration.

In continuum mechanics we can consider a body as set of particles, defined by the position vector X and material configuration β_0 of body at initial time t_0 (material configuration) and position vector x and configuration β_t at certain time t (spatial configuration).

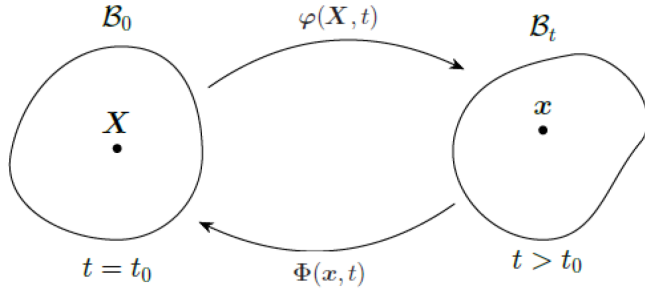


Figure 2.2: Configurations of body in motion

configurations and motion of a body (figure 2.2)

We define a nonlinear deformation map φ , which describes the motion of the body. The deformation map has to be unique, continuous and differentiable and maps the points X in the material configuration to the places x in the spatial configuration

$$x = \varphi(X, t) \text{ with } \varphi: \beta_0 \rightarrow \beta_t \quad (2.16)$$

This description is common in solid mechanics and is denoted as the Lagrangian description of motion: the motion is characterized with respect to the material coordinates and one follows the movement of a particle in time. Inverse mapping is described using

$$X = \varphi(x, t), \text{ with, } \varphi: \beta_t \rightarrow \beta_0 \quad (2.17)$$

Using Lagrangian description displacement field u can be determined as the difference of spatial and material coordinate system.

$$u(X, t) = x(X, t) - X \quad (2.18)$$

Kinetics [4]

The derivation of the kinetic formulation for FE structure is based on the above described principle of structural displacement and D'Alembert principle in Lagrangian formulation.

According to D'Alembert principle the sum of the virtual work of all forces acting on the body must be zero. Hence, the sum of the virtual work of the inertial forces, the internal forces and the applied external body force over an arbitrary volume V_0 , and the applied surface force over an infinitesimal area A_0 of V_0 equals zero, i.e.

$$-\int_{V_0} \delta u^T \rho_0 \ddot{u} dV_0 - \int_{V_0} \delta \epsilon^T H \varepsilon dV_0 + \int_{V_0} \delta u^T b_0 dV_0 + \int_{A_0} \delta u^T p_0 dA_0 = 0 \quad (2.19)$$

let ρ_0 represent the material density, b_0 the vector of the applied external body force over V_0 , p_0 the vector of the applied external surface force over A_0 and the strain tensor. The term H is the, so called, material matrix defined for homogeneous, elastic and isotropic materials, with which the material law is described.

The substitution of Eq.(2.18) into the first summand of Eq.(2.19) leads to the following series of equations:

$$\int_{V_0} \delta u^T \rho_0 \ddot{u} dV_0 = \delta z_F^T \sum_{e=1}^{n_E} \sum \left(T^{eT} \int_{V_0^e} N^{eT}(x) \rho_0^e(x) N^e(x) dV T^e \right) \ddot{z}_F \quad (2.20)$$

$$= \delta z_F^T \sum_{e=1}^{n_E} \sum T^{eT} M^e T^e \ddot{z}_F \quad (2.21)$$

$$= \delta z_F^T M_F \ddot{z}_F \quad (2.22)$$

where,

$$M^e = \int_{V_{0e}} N^{eT}(x) \rho^e(x) N^e(x) dV$$

represents mass matrix for each element of FE structure.

$$M_F = \sum_{e=1}^{n_E} T^{eT} M^e T^e$$

represents mass matrix for entire FE structure.

The substitution of Eq.(2.18) and linearized strain-displacement relation in the second summand of Eq.(2.19) leads to the following:

$$\int_{V_0} \delta \varepsilon^T H \varepsilon dV_0 = \delta z_F^T \sum_{e=1}^{n_E} (T^{eT} \int_{V_{0e}} B^{eT}(x) H^e B^e(x) dV T^e) z_F \quad (2.23)$$

$$= \delta z_F^T \sum_{e=1}^{n_E} T^{eT} K^e T^e z_F \\ = \delta z_F^T K_F z_F \quad (2.24)$$

where,

$$K^e = \int_{V_0} B^{eT}(x) H^e B^e(x) dV$$

represents linear stiffness matrix for each element of FE structure.

$$K_F = \sum_{e=1}^{n_E} T^e K^e T^e$$

represent linear stiffness matrix of whole FE structure.

For the third summand of Eq.(2.19), the definition of the body force for each element of the FE structure is used, using b_0 =Element material density (ρ) * gravity (g)

$$\int_{A_0} \delta u^T b_0 dV_0 = \delta z_F^T \sum_{e=1}^{n_E} (T^{eT} \int_{V_0^e} N^{eT}(x) \rho_0^e(x) dV T^e) g \quad (2.25)$$

$$= \delta \mathbf{z}_F^T \sum_{e=1}^{n_E} \mathbf{T}^{eT} \mathbf{f}_g^e = \delta \mathbf{z}_F^T \mathbf{F}_g \quad (2.26)$$

where,

$$f_g^e = \int_{V_0^e} N^{eT}(x) \rho_0^e(x) dV \Gamma^e g$$

represent body force vector for each element.

$$\mathbf{F}_g = \sum_{e=1}^{n_E} \mathbf{T}^{eT} \mathbf{f}_g^e$$

represent body force vector for whole FE structure.

Finally, for the last summand of Eq. (2.19) the utilization of Eq. (2.18) gives

$$\int_{V_0} \delta \mathbf{u}^T \mathbf{p}_0 dA_0 = \delta \mathbf{z}_F^T \sum_{e=1}^{n_E} \mathbf{T}^{eT} \int_{V_0^e} \mathbf{N}^{eT}(\mathbf{x}) \rho_0^e(\mathbf{x}) dA \Gamma^e \quad (2.27)$$

$$= \delta \mathbf{z}_F^T \sum_{e=1}^{n_E} \mathbf{T}^{eT} \mathbf{f}_p^e = \delta \mathbf{z}_F^T \mathbf{F}_p \quad (2.28)$$

where,

$$\mathbf{f}_p^e = \int_{V_0^e} \mathbf{N}^{eT}(\mathbf{x}) \rho_0^e(\mathbf{x}) dA \Gamma^e$$

represent external applied on surface of each element.

$$\mathbf{F}_p = \sum_{e=1}^{n_E} \mathbf{T}^{eT} \mathbf{f}_p^e$$

represent external force applied on surface of whole FE structure.

Gathering Eq. (2.22), (2.24), (2.26), and (2.28) and substituting them in Eq. (2.19) leads to

$$\delta \mathbf{z}_F^T (\mathbf{M}_F \ddot{\mathbf{z}}_F + \mathbf{K}_F \mathbf{z}_F + \mathbf{F}_g + \mathbf{F}_p) = 0 \quad (2.29)$$

which is general second order LTI equation of motion for undamped FE structure.

If damping effects are to be considered, the definition of the associated parameter is essential. The simplest, and most commonly used, damping model assumes the damping to be linearly proportional to the structure's velocity. This leads to the following equation for linearly damped FE structures in matrix form

$$\mathbf{M}_F \ddot{\mathbf{z}}_F + \mathbf{D}_F \dot{\mathbf{z}}_F + \mathbf{K}_F \mathbf{z}_F = \mathbf{F} \quad (2.30)$$

with \mathbf{D}_F being the structural damping matrix and $\mathbf{F} = \mathbf{F}_g + \mathbf{F}_p$ used for total force acting on structure. The elemental damping can be formulated in similar pattern as for other matrix described above.

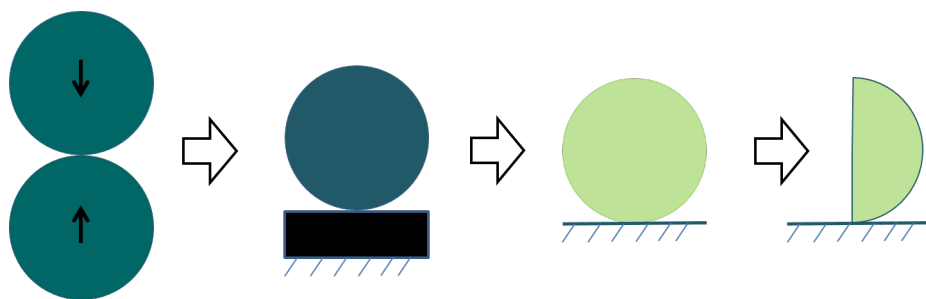
From now on we will drop the suffix F used to represent system matrix and vectors of FE structure, so equation can be written as

$$\mathbf{M} \ddot{\mathbf{z}} + \mathbf{D} \dot{\mathbf{z}} + \mathbf{K} \mathbf{z} = \mathbf{F} \quad (2.31)$$

2.2 Simulation Setup

2.2.1 Sphere vs Rigid Plane

In this simulation the collision of two elastic spheres is studied. Both the spheres have the same magnitude of velocity but opposite directions. As newtons third law of motion states "For every action, there is an equal and opposite reaction", to simplify the model and computation, instead of simulating two spheres colliding, a single sphere colliding against a rigid plane can be simulated. This setup would be equivalent to the original problem as both the spheres are the same in all aspects except for having different directions of velocities.



2.2.2 Symmetry

To further simplify the model, instead of considering the complete sphere, only a 2D semi-circular cross-section is considered. As the spheres are symmetric about the central rotational axis and the angle of contact is 90 degrees, there would not be any velocity in the Y direction.

2.2.3 Mesh

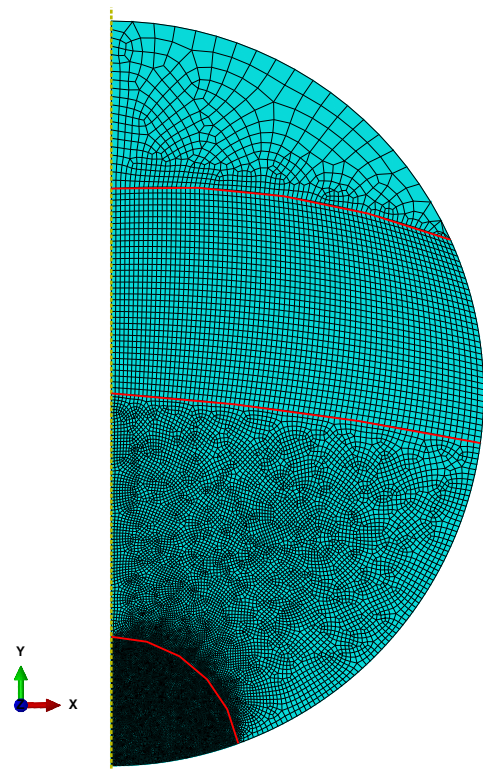


Figure 2.3: Mesh

To create this setup Abaqus CAE provides an option to create axis-symmetric model. The figure 2.3 shows the mesh used in the simulation. A good mesh for this simulation would have to be finer at the bottom i.e. closer to the surface of contact. To create this mesh, the semicircle was divided into four sections. The section closer to the surface of contact has a finer mesh and the region away from the contact surface has a coarse mesh. In figure 2.3 we see the four partitions and the section of the surface of contact has a very fine mesh and the region away from the surface of contact has a coarse mesh.

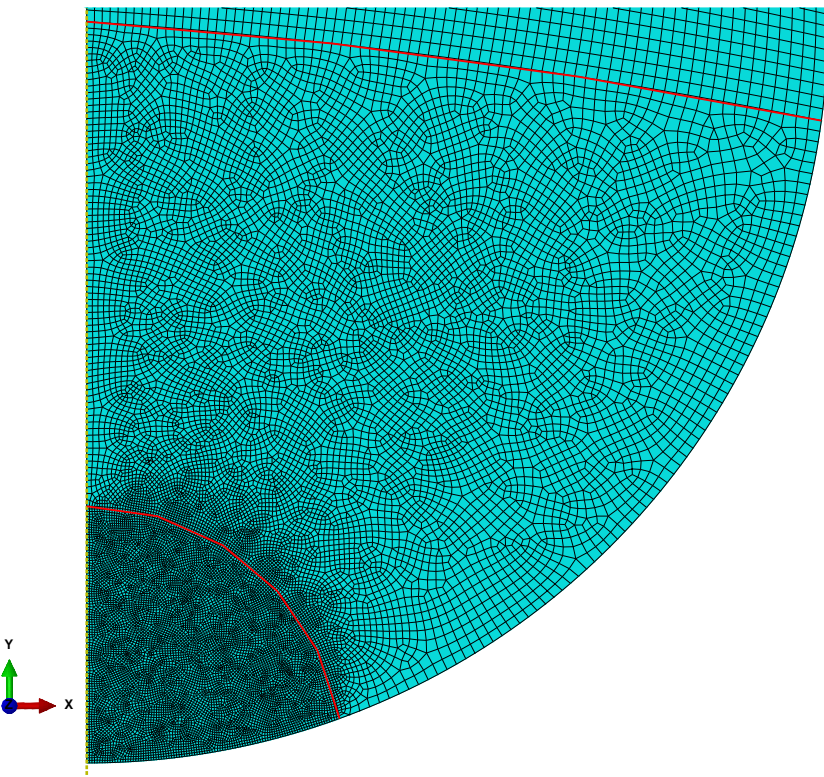


Figure 2.4: Bottom Half of Mesh

The figure 2.4 shows an enlarged image of the bottom half of the mesh. We can see the degree of fineness of the mesh compared to the other half of the sphere.

2.2.4 Rigid Plane

The figure 2.5 shows the rigid plane against which the sphere would be colliding. This plane is an axisymmetric, analytical rigid surface. Analytical rigid surfaces are geometric surfaces with profiles that can be described with straight and curved line segments. These profiles can be swept along a generator vector or rotated about an axis to form a three-dimensional surface. An analytical rigid surface does not contribute to the rigid body's mass or inertia properties.



Figure 2.5: Rigid Plane

2.2.5 Assembly

The final assembly is of the sphere in contact with the rigid plane as shown in figure 2.6. The sphere is given a velocity in the $-y$ direction. The starting point of the simulation is when the sphere is in contact with the plane and is about to collide with the plane.

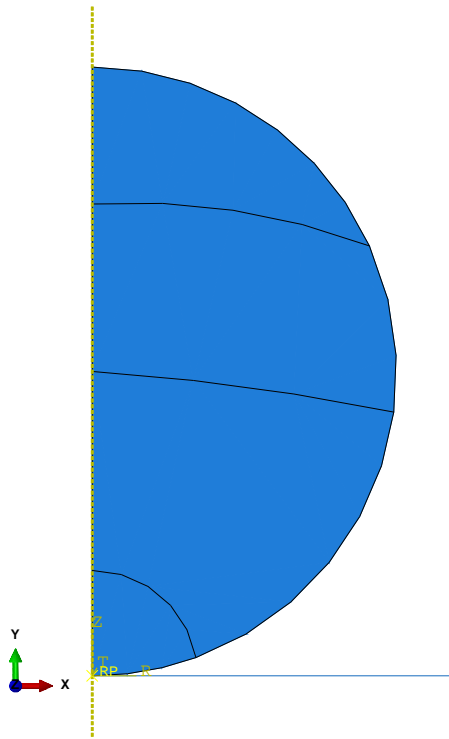


Figure 2.6: Assembly

2.3 Measurement Quantities

2.3.1 Displacement

To measure the displacement of the body, the displacement of the center of mass was measured. The center of mass of the sphere is located at the geometric center of the sphere. The figure 2.7 shows the center of the 2D semi-circle in red, which was considered as the sphere of the model. To measure the displacement center of mass of the sphere, the displacement of center of the semicircle was considered.

2.3.2 Kinetic Energy

The kinetic energy of an object is the energy that it possesses due to its motion. It is expected that some of the kinetic energy will be converted to strain energy, which can be seen by vibrations in the sphere. The kinetic energy will also be used to calculate the coefficient of restitution of the sphere for various impact velocities.

$$\text{KineticEnergy}(KE) = \frac{mv^2}{2} \quad (2.32)$$

where m is the mass of the object and v is the velocity of the object.

2.3.3 Strain Energy

The strain energy is the energy stored by a system undergoing deformation. During a collision, a part of the kinetic energy is converted into strain energy. This conversion of kinetic energy to strain energy is ignored due to the quasi static assumptions. This strain energy can also be observed as vibration on the body of the object. When the load is removed,

$$\text{StrainEnergy}(U) = \frac{V\sigma\epsilon}{2} \quad (2.33)$$

where V is volume, σ is stress and ϵ is strain.

2.3.4 Coefficient of Restitution

The coefficient of restitution is an effective method of understanding the loss of energy in a body during collisions. The coefficient of restitution is a measure of the restitution of kinetic energy after the collision of two objects. The coefficient of restitution is calculated by,

$$COR = \frac{-\text{Velocity after impact}}{\text{Velocity before impact}} \quad (2.34)$$

2.4 Verification

To verify the correctness of the simulation setup, various meshes were tried. As Abaqus CAE has an option to automatically choose a suitable timestep, the automatic option was chosen. The validity of considering a a 2D semi circle instead of a complete sphere was check by confirming the mass of the model in the to the calculated mass of the sphere of the same material.

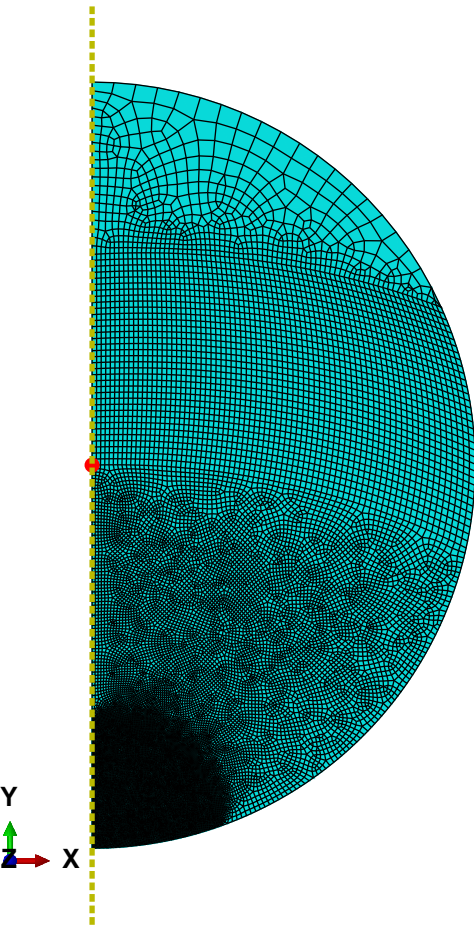
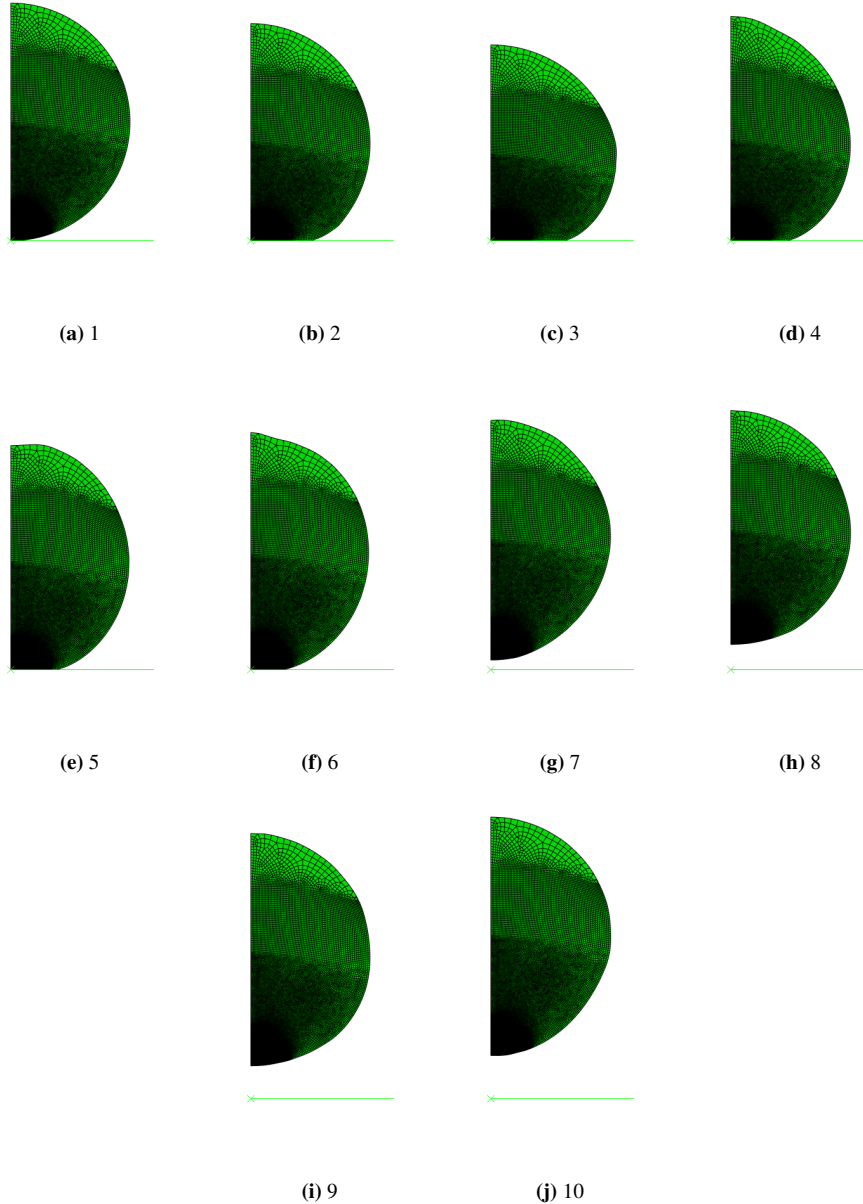


Figure 2.7: Center of sphere

3

RESULTS

3.1 Results

**Figure 3.1:** A very soft material

As we study the loss of kinetic energy to vibrations let's first consider a very soft material. The series of figures in 3.1 shows the trajectory of a very soft material with Young Modulus(E)= 6 MPa with an impact velocity of 5 m/s. After the contact is lost, spheres starts to vibrate violently. This shows that some part of the kinetic energy possessed by the sphere is converted to strain energy which then caused the vibrations in the sphere.

3.1.1 Contact Force

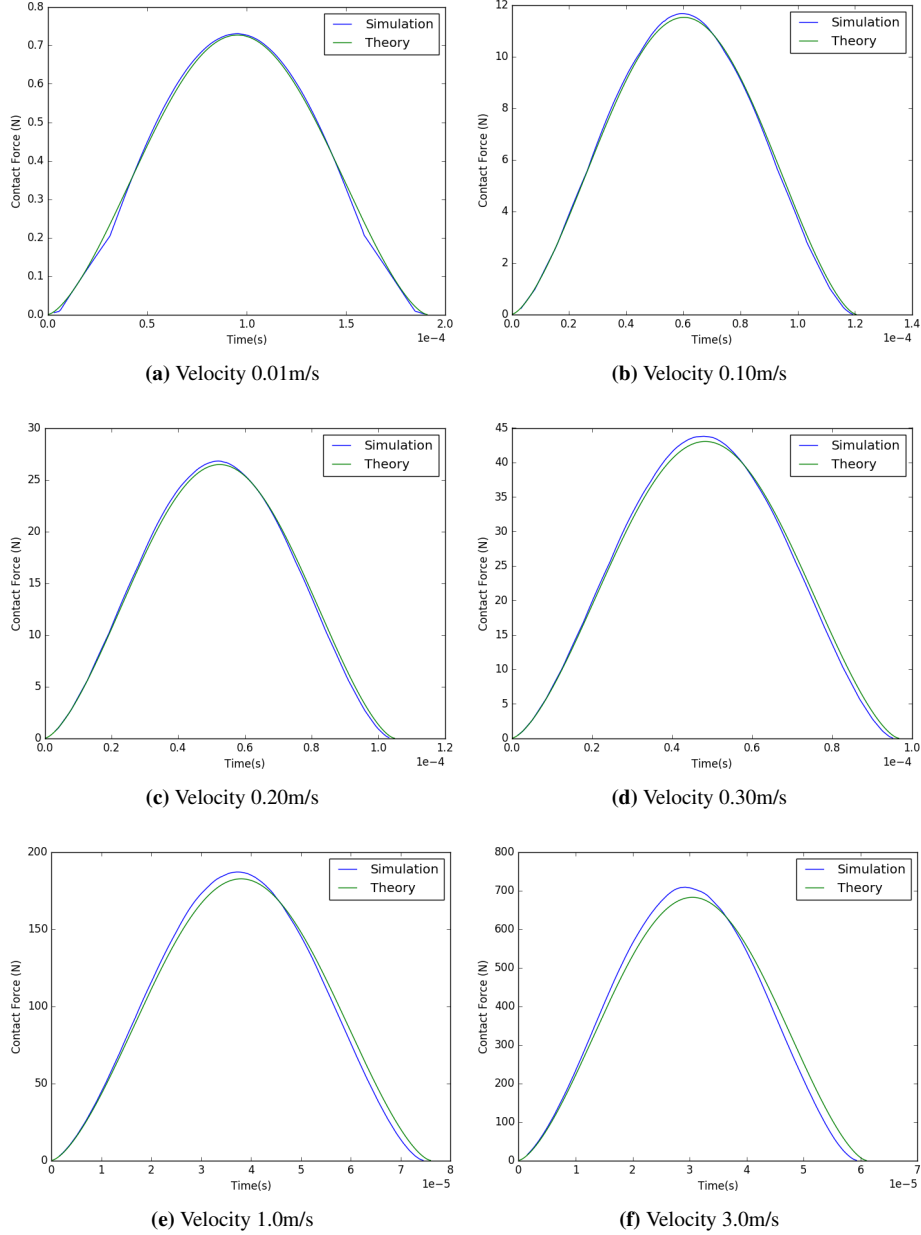


Figure 3.2: Contact force vs Time for various impact velocities

Now considering a harder material, i.e. with Young's Modulus(E) of 9.3GPa and mass density of 900Kg/m^3 . This Young's Modulus was chosen as it was neither too hard nor too soft and had the vibration visible. The plots in figure 3.2 show the contact force between the sphere and the rigid plane. The plots shows that as the impact velocities are higher, the difference between the simulation data and the theoretical data is more visible. This errors is due the quasi static assumptions.

3.1.2 Deformation

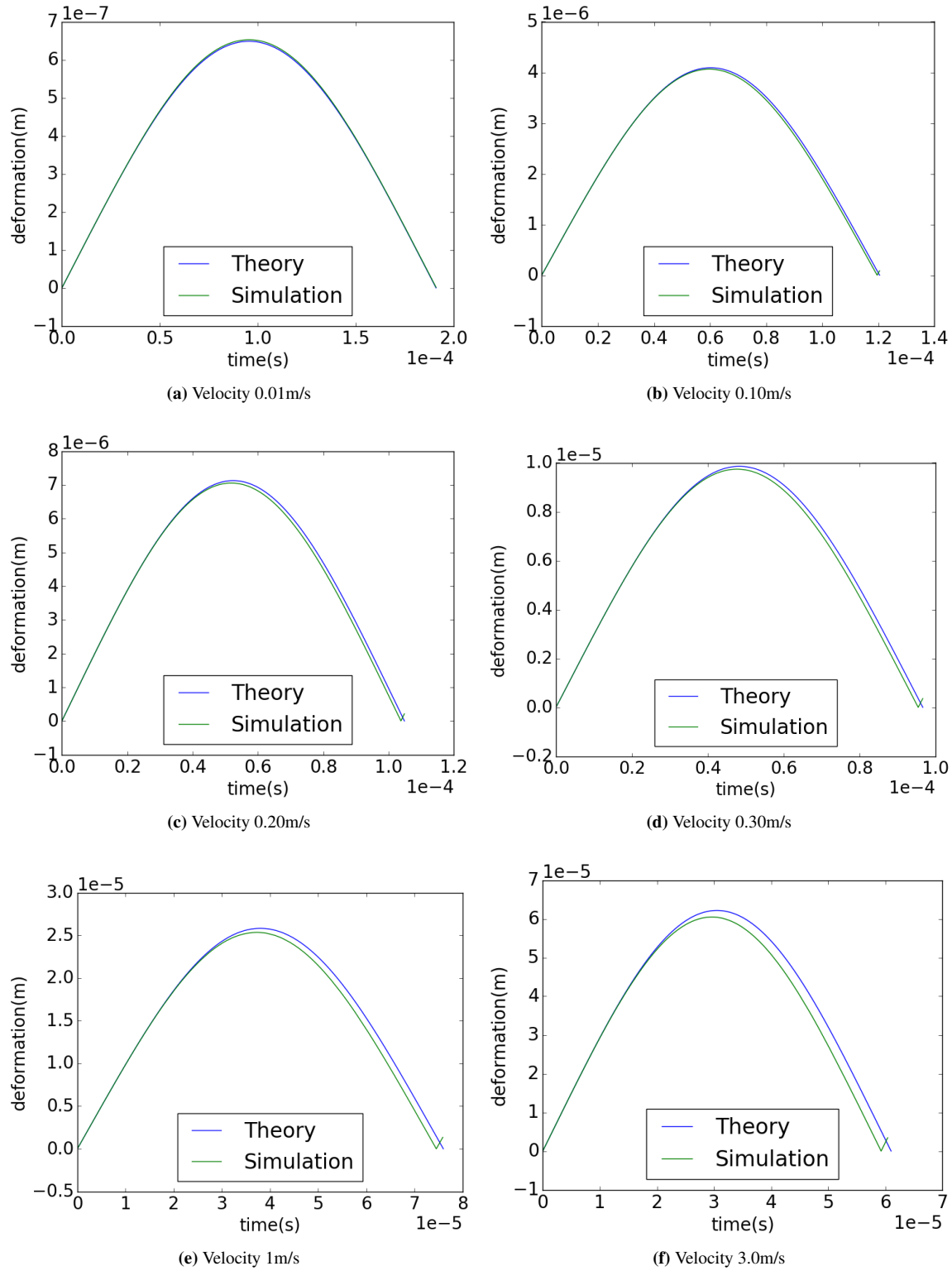


Figure 3.3: Displacement of the center of the sphere for various impact velocities

The plots in figure 3.3 show displacement of the center point of the sphere with respect to time. The plots shows that as the impact velocities are higher, the difference between the simulation data and the theoretical data is more visible. This errors is due the quasi static assumptions. But unfortunately these plot are not conclusive as the velocity of the center of mass is the velocity which should be compared and not the velocity of the center of the sphere.

3.1.3 Energy

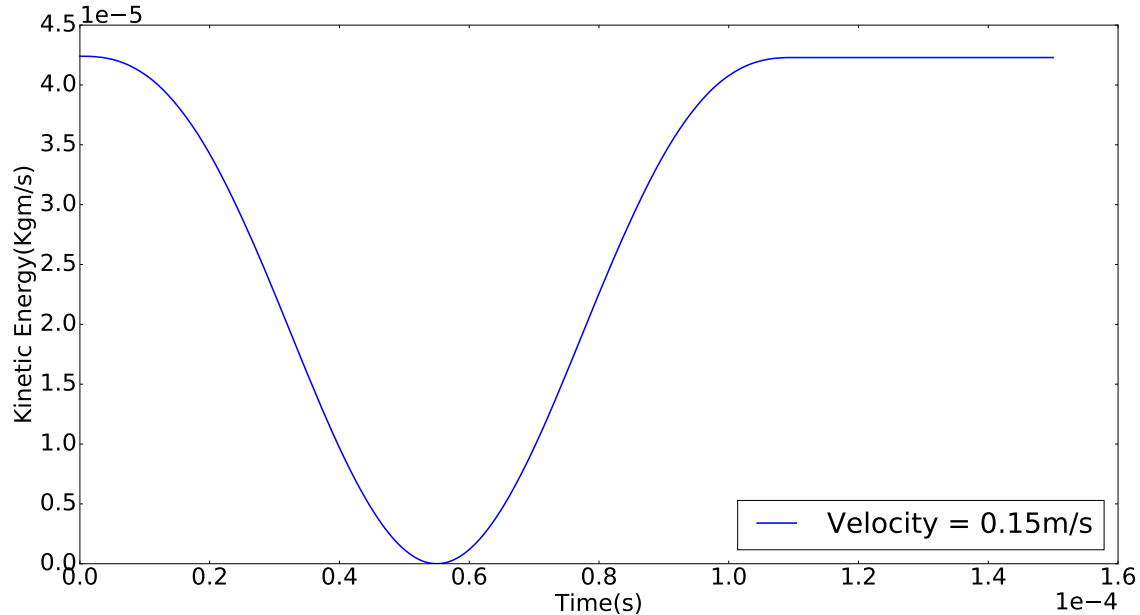


Figure 3.4: Kinetic Energy

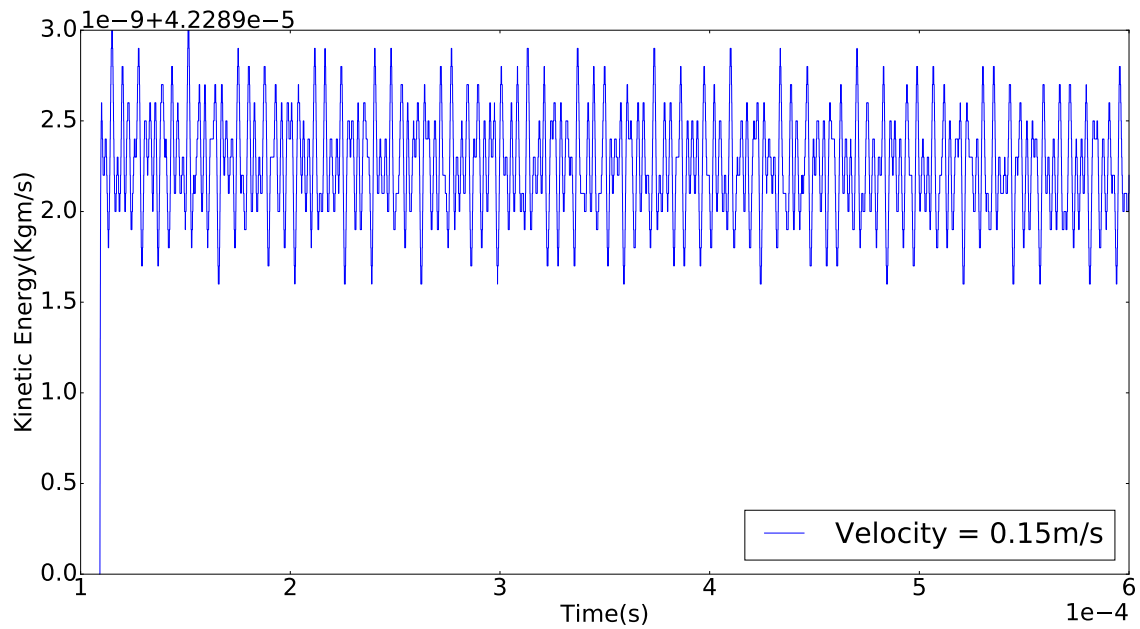


Figure 3.5: Kinetic Energy contact after impact

The figure 3.4 shows Kinetic Energy vs Time for the impact velocity of 0.15m/s . It is clear that the kinetic energy decreases in the beginning of the impact and increases towards the end of the impact. When observed carefully, fluctuations can be observed in the plot after the impact is completed as shows in figure 3.5. As discussed in the previous paragraphs, this is because a part of the kinetic energy is converted into strain energy which cause vibrations in within the model.

A similar trend is also visible in the plot of the strain energy of the sphere. It is clear from figure 3.7, that after the collision is complete, the body still possesses a small amount of strain energy.

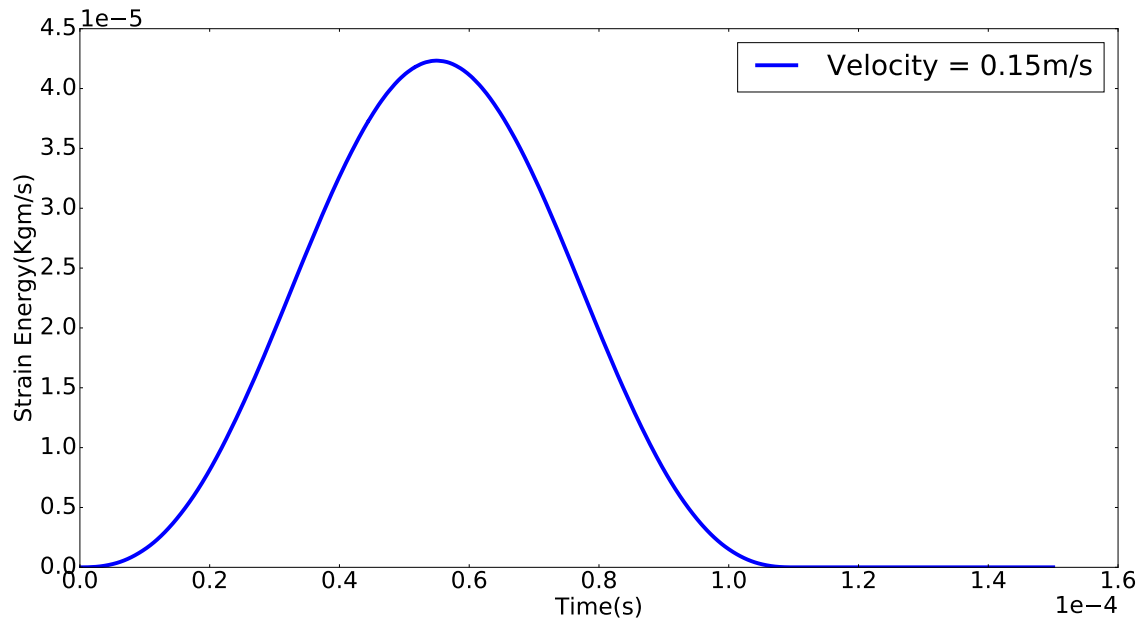


Figure 3.6: Strain Energy

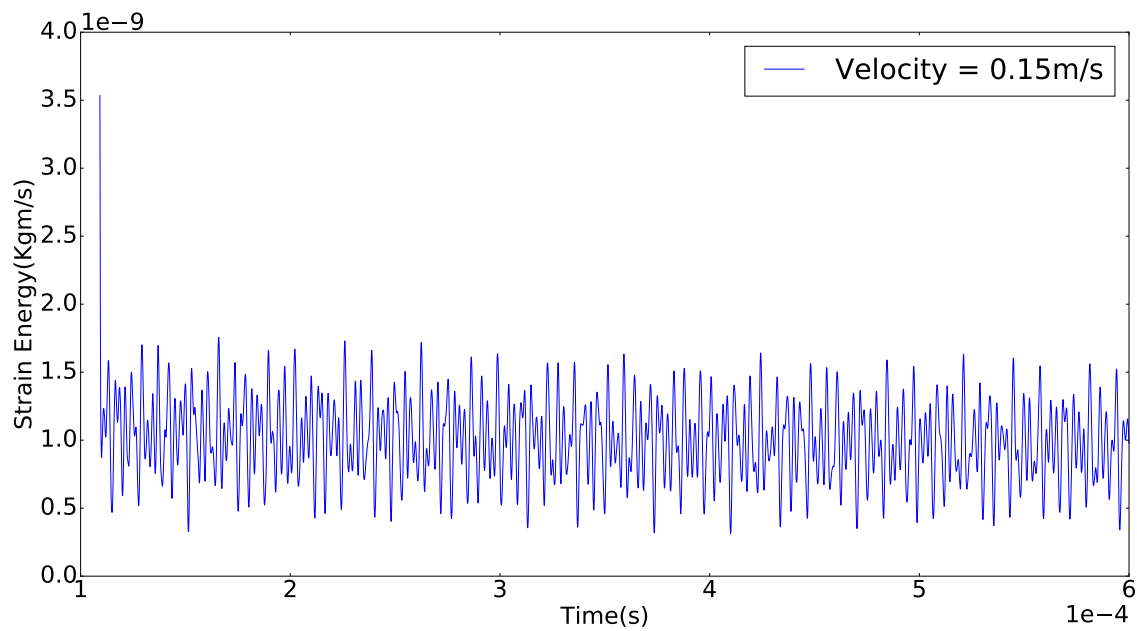


Figure 3.7: Strain Energy after contact is broken

3.1.4 Coefficient of Restitution

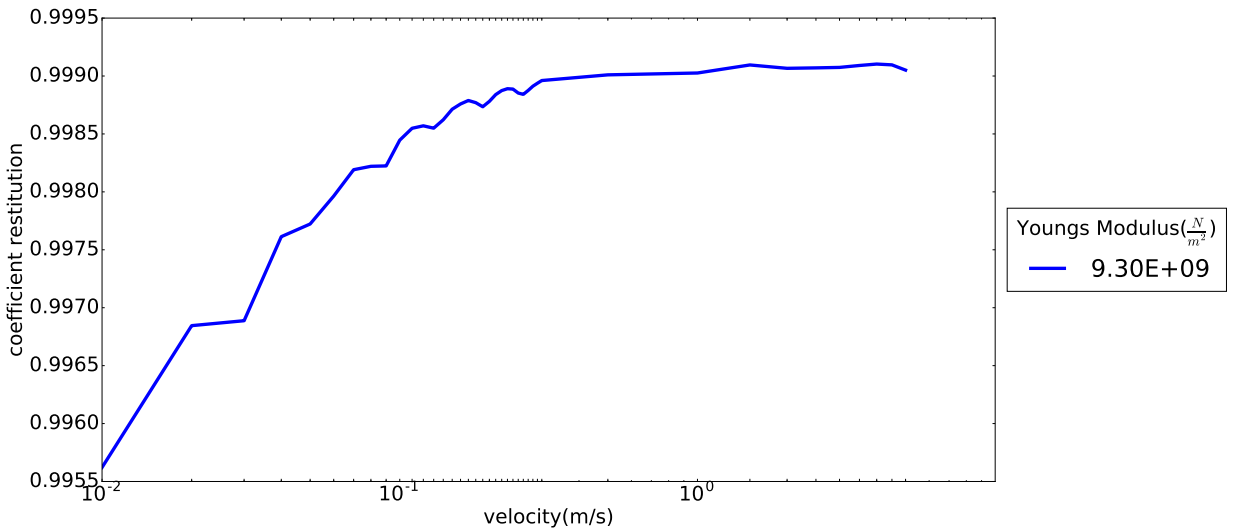


Figure 3.8: Coefficient of restitution

To understand the loss of energy to vibrations, the coefficient of restitution was calculated for an elastic material with *YoungsModulus*(E) of $9.3GPa$ and various impact velocities ranging from $0.01m/s$ to $5m/s$. The coefficient of restitution was calculated by,

$$COR = \sqrt{\frac{\text{Kinetic Energy after impact}}{\text{Kinetic Energy before impact}}} \quad (3.1)$$

Kinetic Energy was used to calculate the coefficient of restitution because, calculating trajectory of the center of mass of the model was much more computationally intensive and inaccurate than calculate the Kinetic energy of the complete. Measure the coefficient of restitution is a measure of the restitution of kinetic energy after the collision of two objects. The figure 3.8 shows the coefficient of restitution vs various impact velocities. We can see that the coefficient of restitution increases as the impact velocities are increased. The bumps in the plot can be explained after performing a Fourier analysis on the models. The Fourier analysis shows that the bumps correspond to the eigen modes of the model.

3.1.5 Modal Analysis

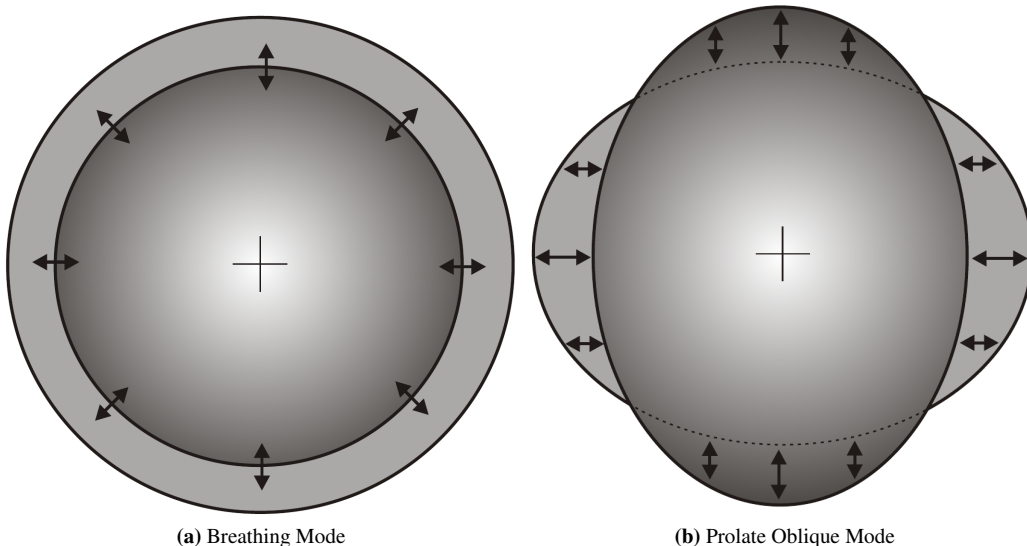


Figure 3.9: Different modes of vibration

To understand the plot in figure 3.8, the modal analysis of the sphere was necessary. The natural frequencies of the sphere can affect the trajectory of the sphere during the impact. The two natural modes are shown in figure 3.9.

The modes shown in figure 3.9 can affect the velocity of the sphere after the impact is complete. For example, when the sphere is in the prolate mode towards the end of the impact, the velocity of the sphere increases as the direction of the velocity of the sphere and the natural vibration modes are the same and decreases if the sphere is in the oblate mode during the end of the impact.

Eigen Frequencies of an elastic sphere

Breathing Mode Using equation from the book "A Treatise on the Mathematical Theory of Elasticity" by A.E.H. Love, chapter 11:Vibration of spheres [3].

$$\frac{h_a}{\pi} = 0.8160 = \frac{\frac{2R}{v_{dil}}}{T_{os}} \quad (3.2)$$

$$v_{dil} = \sqrt{\frac{\lambda + 2\mu}{\rho}}$$

where $\frac{\pi}{h_a}$ is the ratio of the period of oscillation of the time taken by a wave of dilation to travel over a distance equal to the diameter of the sphere, v_{dil} is the velocity of the wave of dilation, R is the radius of the sphere, T_{os} is the time period of 1 oscillation, λ and μ are the lame's constants and ρ is the mass density.

$$T_{os} = \frac{1}{F} = \frac{2R}{v_{dil}} \frac{\pi}{h_a} = \frac{2R}{v_{dil}} \frac{1}{0.8160} \quad (3.3)$$

Poissons condition $\Rightarrow \lambda = \mu \Rightarrow \nu = \frac{1}{4}$

Therefore,

$$v_{dil} = \sqrt{\frac{3\lambda}{\rho}} \quad (3.4)$$

and since

$$\lambda = \nu \frac{E}{2(1+\nu)} = \frac{E}{2(\frac{5}{4})} = \frac{2E}{5} \quad (3.5)$$

v_{dil} now becomes

$$v_{dil} = \sqrt{\frac{6E}{5\rho}} \quad (3.6)$$

we now have a equation for T_{os}

$$T_{os} = 2R \sqrt{\frac{5\rho}{6E}} \frac{1}{0.8160} \quad (3.7)$$

For $R = 0.01m$, $E = 9.3Gpa$ and $\rho = 900kg/m^3$

$$T = 2 \times 0.01 \sqrt{\frac{5 \times 900}{6 \times 9.3 \times 10^9}} \frac{1}{0.8160} = 0.00000696031s \quad (3.8)$$

$$F = \frac{1}{T} = 143671.625591Hz \quad (3.9)$$

Prolate Oblate Mode Again using equation from the book "A Treatise on the Mathematical Theory of Elasticity" by A.E.H. Love, chapter 11:Vibration of spheres [3].

$$\frac{\kappa_a}{\pi} = \frac{\frac{2R}{v_{dist}}}{T_{os}} = 1.8346 \quad (3.10)$$

where $\frac{\pi}{\kappa_a}$ is the ratio of the period of oscillation to the time taken by a wave of distortion to travel over a distance equal to the diameter of the sphere and v_{dist} is the velocity of the wave of distortion.

$$v_{dist} = \sqrt{\frac{\mu}{\rho}} = \sqrt{\frac{2E}{5\rho}} \quad (3.11)$$

$$T = \frac{2R}{\sqrt{\frac{2E}{5\rho}} \times 1.8346} = 2R \sqrt{\frac{5\rho}{2E}} \frac{1}{1.8346} \quad (3.12)$$

For $R = 0.01m$, $E = 9.3Gpa$ and $\rho = 900kg/m^3$

$$T = 2 \times 0.01 \sqrt{\frac{5 * 900}{2 * 9.3 * 10^9}} \frac{1}{1.8346} = 0.00000536214s \quad (3.13)$$

$$F = \frac{1}{T} = 186492.602141 \text{ Hz} \quad (3.14)$$

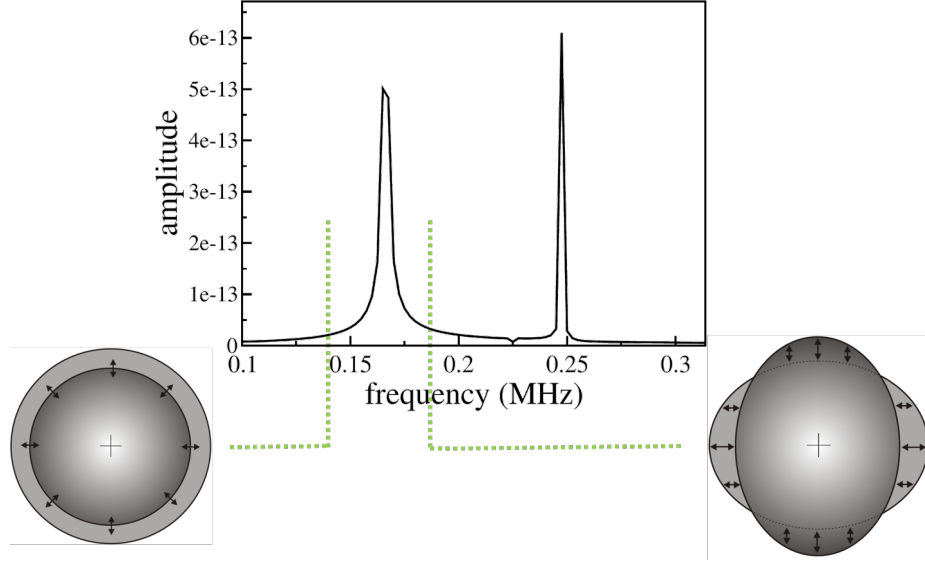


Figure 3.10: Fourier Transform of Strain Energy

Now performing a fourier transform on the data of the strain energy remaining in the sphere after the impact is complete the frequency spectrum shown in figure 3.10 was obtained.

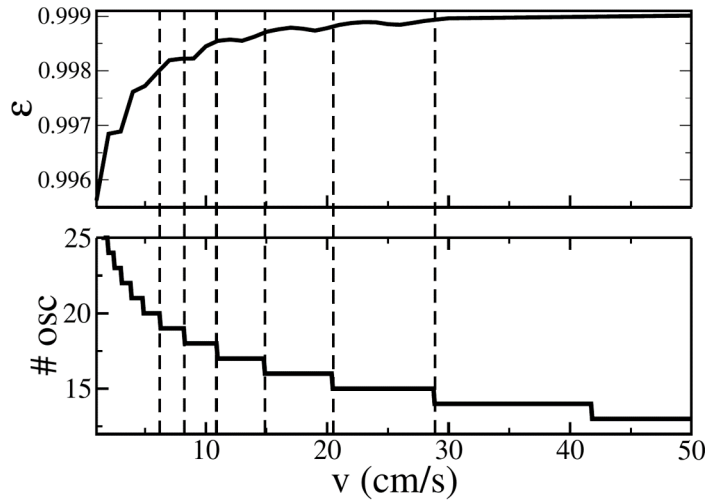


Figure 3.11: Number of oscillation during contact

Now we calculate the number oscillations of the during the time of contact. When the plot of coefficient of restitution and number of oscillation is compared in figure 3.11, we observe whenever the number of completed oscillations increments by 1, the plot in figure 3.8 tends to dip and create a valley. This shows when the sphere is in the oblate phase of the vibration, it results in a higher after impact velocity, hence create a bump in the plot of the coefficient of restitution.

3.2 Parametric Study

The next step of further study would be to study how various parameters such as material and diameter of the sphere would effect the above obtained results.

3.2.1 Different Young's Modulus

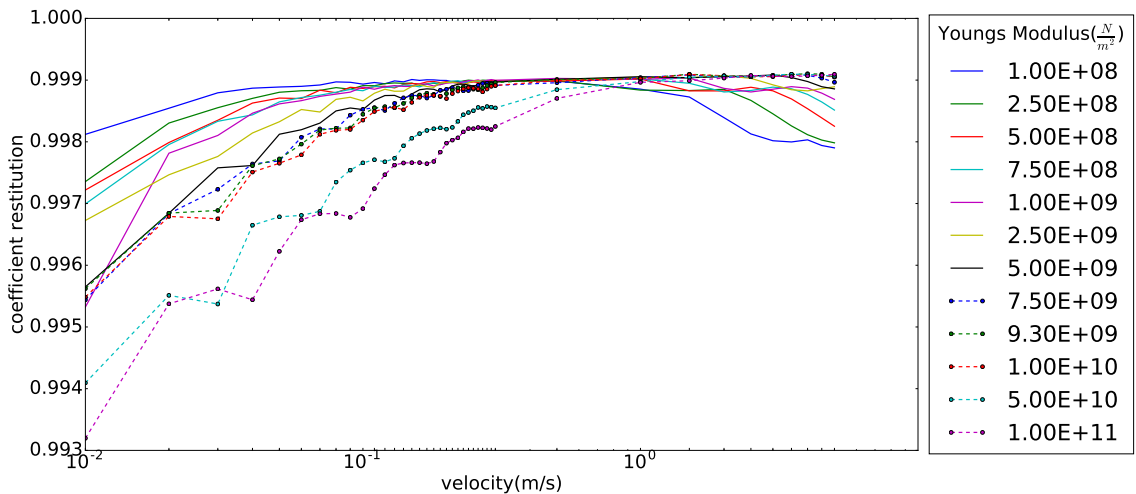


Figure 3.12: Coefficient of restitution for various Young's Modulus

The simulation was performed for a range of Young's Moduli ranging from $1e8 N/m^2$ to $1e11 N/m^2$. It can be observed from the plots in figure 3.12, for higher velocities as the E increases the COR saturates to a level, which implies for materials for higher E , the percentage loss of kinetic energy remain constant. Whereas for lower velocities we see the reverse plots, i.e higher E 's have a lower coefficient of restitution. This results was unexpected as the expected result was a gradual increase in coefficient of restitution as the E increases.

3.2.2 Different Diameters

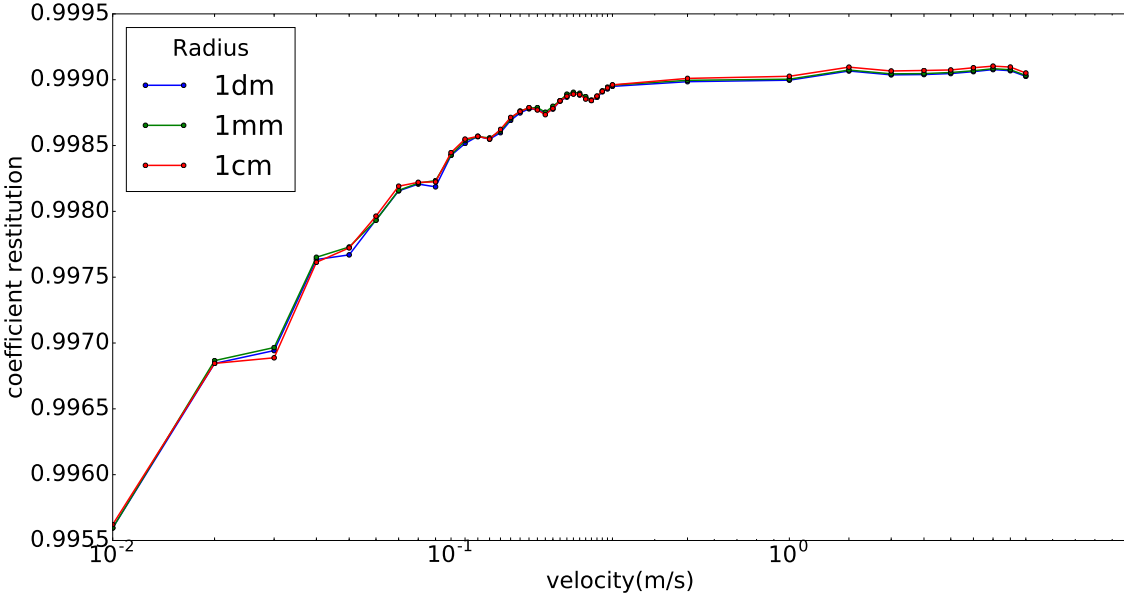


Figure 3.13: Coefficient of restitution for various radii

The simulation was also performed for various spheres of diameters of $0.001m$, $0.01m$ and $0.1m$. Considering the equations for coefficient of restitution from [5] for viscoelastic spheres .

$$\varepsilon = 1 + \sum_{k=0}^{\infty} h_k (\beta^{\frac{1}{2}} v^{\frac{1}{10}})^k$$

where

$$\begin{aligned}\beta &= \frac{3}{2} A \left(\frac{\rho}{m_{eff}} \right)^{\frac{2}{5}} \\ \beta &\propto \left(\frac{\rho}{m_{eff}} \right)^{\frac{2}{5}}\end{aligned}$$

also

$$\rho \propto \sqrt{R}, \quad m_{eff} \propto R^3$$

therefore

$$\beta \propto \left(\frac{\sqrt{R}}{R^3} \right)^{\frac{2}{5}} = R^{-\frac{1}{5}}$$

Hence we see, for a viscoelastic case the coefficient of restitution is inversely proportional to the radius. A similar result was expected for the elastic case, but the plot in figure 3.13 does not agree. We see there is no effect of diameter on the coefficient of restitution in the elastic case.

4

CONCLUSION AND FUTURE WORK

4.1 Summary

In this thesis the validity of the current force model used in simulation of granular materials was challenged. The current theory for contact problems for elastic and viscoelastic materials involve quasi static approximations. The quasi static assumptions imply that the characteristic deformation rate is much smaller than the speed of sound in the material and that the relaxation time of the particle's material is negligible compared to the duration of the contact. The validity of these assumptions is probed by considering the case of impact between two elastic spheres. The simulations were preformed using the Finite Element tool Abaqus CAE.

To validate the quasi static assumptions various quantities such as deformation, contact force and coefficient of restitution were studied. The plots of deformation do show an error between the theory and the simulation for higher impact velocities, but a more convincing quantity to determine the effect of the assumptions was the coefficient of restitution, which was calculated using the kinetic energy of the sphere before and after the impact. These results show the loss of kinetic energy in the sphere, which was converted to strain energy resulting in vibrations within the sphere. The loss of kinetic observed in the simulations was much smaller than expected, hence the quasi static assumption are valid. A modal analysis was also conducted to further verify the nature of the coefficient of restitution vs impact velocity plot, which are affected by the natural vibrations of the sphere.

A parametric study was also conducted by varying the Young's Modulus and diameter of sphere. In the case of the varying Young's Modulus, the coefficient of restitution seems to reach a maximum value for higher Young's Moduli, whereas the variation of the radius of the sphere did not results in any change in the plots, which was unexpected as for viscoelastic materials the coefficient of restitution is inversely proportional to the radius of the sphere.

4.2 Future Work

The conditions of an elastic material and two spheres colliding normally are not possible or improbable in real world scenarios. This work can further be extended to study more real world conditions such as

Tangential interaction

In this study, a normal interaction was considered, but in a real world situations such interactions are rare. Granulates can collide at in any direction and velocity.

Non spherical particles

Granulates generally are not spherical and come in various shapes and sizes. This study can be further extended to granulates of different shapes interacting at different angles and velocities.

Viscoelasticity and Plasticity

This study was focused on purely elastic materials, but not all matter found in nature can be considered as elastic. Further studies can be conducted considering viscoelastic and plastic materials.

Multi-particle Interaction

Granular materials such as sand, snow and powders can consist of thousands of granulates and in scenarios such as landslides and snow storms can have collisions from multiple particles at a time.

4

BIBLIOGRAPHY

- [1] Jacques Duran. *Sands, Powders, and Grains: An Introduction to the Physics of Granular Materials (Partially Ordered Systems)*. Springer, 1999. ISBN 0387986561.
- [2] L. D. Landau and E. M. Lifshitz. *Theory of Elasticity*.
- [3] A. E. H. Love. *A treatise on the mathematical theory of elasticity*.
- [4] Julia Mergheim. Lecture notes nonlinear finite element. LTM, FAU Erlangen.
- [5] Patric Muller and Thorsten Pöschel. *Collision of viscoelastic spheres: Compact expressions for the coefficient of normal restitution*. Physical Review E 84, 021302, 2011.
- [6] Thorsten Pöschel and T. Schwager. *Computational Granular Dynamics - Models and Algorithms*. Springer, 2005. ISBN 978-3-540-27720-0.

